buildings

MDPI

Article

Time-Dependent Behavior of Ultra-High Performance Concrete Beams under Long-Term Bending Loads

Jiayue Li [1], Yankai Lu [1], Xiaorui Jia [1], Bo Liu [1,*], Juannong Chen [1] and Qingjuan Meng [2]

[1] College of Civil and Architectural Engineering, North China University of Science and Technology, Tangshan 063210, China; lijiayue@ncst.edu.cn (J.L.); luyankai1999@outlook.com (Y.L.); jxiaorui0116@outlook.com (X.J.); chenjuannong@ncst.edu.cn (J.C.)
[2] School of Civil Engineering, Tangshan University, Tangshan 063000, China; mqj27@outlook.com
* Correspondence: liubo19840311@ncst.edu.cn

Abstract: In the past, scholars have studied the creep of UHPC, mainly in compression and tension but not bending creep. In this research, 20 ultra-high performance concrete (UHPC) beams were tested for bending creep under long-term loading, and the changes of beam deflection, temperature, and humidity with time were obtained for 445 days of continuous loading. The deflection patterns of UHPC beams with time were analyzed for different steel fiber content, curing systems, water/binder ratio, sand/binder ratio, and stress levels. The results showed that steel fiber had an obvious inhibition effect on initial deflection, but a dosage of steel fiber too high would offset part of the inhibition effect of steel fiber on creep. The use of heat treatment had a better inhibition of creep in the later stage of UHPC, but heat treatment must be matched with necessary moisture content, and hot water maintenance was the most efficient. Both a high water/binder ratio and high stress level increased the bending creep of the specimen. Bending creep increased with the increase in the sand/binder ratio. Therefore, attention should be paid to the total amount and ratio of cementitious materials and fine aggregates in UHPC.

Keywords: UHPC; steel fiber; bending creep; heat treatment; water/binder ratio

Citation: Li, J.; Lu, Y.; Jia, X.; Liu, B.; Chen, J.; Meng, Q. Time-Dependent Behavior of Ultra-High Performance Concrete Beams under Long-Term Bending Loads. *Buildings* **2024**, *14*, 1761. https://doi.org/10.3390/buildings14061761

Academic Editor: Francesco Ascione

Received: 9 May 2024
Revised: 29 May 2024
Accepted: 6 June 2024
Published: 11 June 2024

1. Introduction

All concrete structures experience time-dependent deformations known as shrinkage and creep. Shrinkage is a reduction in volume due to the evaporation of water or a chemical reaction within the concrete, independent of external loading. Creep is the increasing deformation of concrete under sustained stress in the direction of the applied load. Shrinkage and creep are inherent properties of concrete, and both significantly affect the long-term performance of structures, especially in large structures. Therefore, it is of great engineering significance to understand the pattern of change of shrinkage and creep of concrete materials.

In order to assess tensile and bending creep, Ranaivomanana et al. [1] created a test setup. They compared basic creep at the three stress levels with various loading modes and provided findings from experiments that were subjected to sustained stresses of 30%, 40%, and 50% of tensile or compressive strength. Babafemi et al. [2] reported delayed cracking of cracked concrete incorporated with short discrete synthetic fibers under 8 months of service conditions. The tensile creep properties of early age concrete were studied by Liang et al. [3], and they developed a method for calculating incremental tensile creep and enhanced the Kelvin model based on the degree of hydration. In order to evaluate the difference between the creep response of cracked plastic fiber concrete beams and steel fiber concrete beams under bending loads, Pujadas et al. [4] discussed the influence of crack cracking and environmental conditions on the long-term deformation behavior of beams. Jahami et al. [5] investigated the mechanical properties of low-cost, high-strength concrete by partially replacing fine aggregates with waste glass sand. Manjunatha et al. [6]

investigated the freshness, strength properties, microstructure analysis, and environmental impact assessment of an M60 grade self-compacting concrete prepared with silica fumes, ground granulated blast furnace slag, and different proportions of PVC waste powder, and they conducted a full life cycle assessment. Many scholars have also studied the different types of creep of the same type of concrete [7–10] and fiber-reinforced concrete [11–15].

Ultra-high performance concrete (UHPC) is a new cement-based composite material, and it has a dense matrix, a low water/binder ratio, and excellent tensile and compressive strength as well as ductility and durability. Moreover, it has outstanding low permeability, strong resistance to corrosion and carbonation, and strong freeze–thaw stability. In addition, the high volume-doped fibers reinforce the UHPC matrix, resulting in a high tensile capacity even after cracking of the UHPC. Due to its superior mechanical characteristics and longevity, UHPC is being utilized more frequently in pre-stressed bridge building. UHPC provides larger spans and excellent durability for pre-tensioned pre-stressed girders. However, creep and shrinkage deformation are particularly important in pre-stressed beams. Creep and shrinkage can lead to a gradual loss of pre-stress, thereby affecting the load-bearing capacity of components and potentially causing usability issues in the structure. For this reason, accurately estimating the pre-stress loss caused by long-term deformations such as shrinkage and creep is crucial for the design of pre-tensioned UHPC girders.

In recent years, with the wide application of UHPC, many scholars have also conducted a lot of research on the creep properties of UHPC. Fiber optic grating sensors were employed by Yazdizadeh et al. [16] to assess the creep and shrinkage of regular concrete, high-performance concrete, and UHPC. There was a strong link between the creep and shrinkage test findings. Yang et al. [17] conducted an experimental study on the creep performance of NC-UHPC composite columns. The results showed that the creep coefficients of the NC-UHPC composite columns were significantly lower than those of the NC columns. Zhu et al. [18] developed an ABAQUS user subroutine using the recursion of adjacent stress increments in the time history algorithm to simulate the creep shrinkage of plain concrete and UHPC. The long-term performance of UHPC beams, including bending and compression creep, was examined by Llano et al. [19]. Xu et al.'s [20] study examined the compression creep behavior of specimens with water/binder ratios of 0.16 and 0.22 and steel fiber volume levels of 0%, 1%, and 2%. The findings demonstrated that the creep coefficients of 1% and 2% ultrafine steel fibers dropped dramatically by 25.4% and 13.4% after loading for 180 days, respectively, in comparison to the unloaded ones. The creep behavior of UHPC was adversely affected by an increase in the water/cement ratio. The effects of the fiber type and admixture, water-to-cement ratio, and cementitious material content on UHPC shrinkage and creep were examined by Chen et al. [21]. Zhang et al. [22,23] investigated the creep behavior of UHPC creep damage under high uniaxial compressive stresses. Mohebbi et al. [24] measured the compressive creep properties of various UHPC materials, assessed the impact of various environments (such as high, low, and hermetic conditions) on the unconfined shrinkage and compressive creep of various UHPC materials, and created prediction equations.

Many scholars have also studied the creep of UHPC under different heat treatment conditions. Garas [25] studied the effect of fiber content on the compressive creep of UHPC under different heat treatment conditions. The results indicated that heat treatment can improve the creep deformation resistance of steel fibers by increasing the interfacial strength between fibers and the matrix. Garas et al. [26] considered three curing temperatures (23 °C, 60 °C, and 90 °C). The results indicate that the creep of UHPC was mainly determined by the temperature level, rather than the total heat input. Cui [27] designed an experimental program to study the creep behavior of UHPC under various curing schemes, and the results showed that under the combined curing scheme, the creep deformation of UHPC was significantly reduced. Abid et al. [28] investigated the steady-state creep behavior of UHPC at high temperatures. The results indicated that the creep of UHPC at room temperature was comparable and that the steady-state creep increases with the increase in

the load level. The above scholars have considered the effects of various heat treatments on the creep of UHPC, but the types of heat treatments are still limited.

In the past, scholars have studied the creep of UHPC mainly in compression and tension, with limited reports on the bending creep of UHPC. The problem of excessive mid-span deflections exists in bridge engineering, and these excessive deflections and the resulting cracks may lead to poor bridge service quality and a series of durability problems. UHPC has excellent compressive and tensile strength, as well as significant durability, and is increasingly being used in bridge engineering. However, creep and shrinkage have a significant impact on the long-term performance of UHPC. Thus, for the application of UHPC in bridge engineering, it is crucial to comprehend the bending creep features of UHPC.

To study the flexural creep performance of UHPC, an experimental study of the deformation performance of 20 UHPC beams under long-term loading was carried out. The temperature, humidity, and deflection changes of the beams were obtained over a period of 445 days of continuous loading, and the changes in deflection of UHPC beams were analyzed for various steel fiber content, curing systems, water/binder ratio, sand/binder ratio, and stress levels. The results of the experiments can serve as a reference for the computation of UHPC beams' long-term deformation. The test findings can be used as a guide to determine how much UHPC beams will deform over time.

2. Experimental Program

2.1. Test Materials

P·II 52.5R Portland cement specific surface area is 375 m^2/kg. Fly ash 45 μm square hole screening ratio is 9.6%. The SiO_2 content of the silica fume is 94%, and the ignition loss at 950 °C is 1.15%. Mineral powder specific surface area is 419 m^2/kg. The diameter of quartz sand is 0.85–1.7 mm. Superplasticizer was added to obtain appropriate workability. Two types of copper-plated steel fibers (RS65/8) and end-hooked steel fibers (RS60/13) were incorporated into UHPC, with a volume ratio of 1:2 between the two. Steel fiber mechanical properties are shown in Table 1.

Table 1. Steel fiber mechanical properties.

Type	Elastic Modulus/GPa	Tensile Strength/MPa	Diameter/mm	Length/mm	Aspect Ratio	Density/(kg/m^3)
RS65/8	210	2850	0.12	8	65	7800
RS60/13	210	2850	0.22	13	60	7800

The volume mixing rate of steel fibers was 2.0%, the water/binder ratio of UHPC utilized in the reference specimen RS was 0.16, the sand/binder ratio was 1.0, standard maintenance was applied, and the mixing ratios are displayed in Table 2. The reference mix proportion (specimen RS) in this experiment was a mix proportion independently tested and used by our research group for a long time, and its physical properties met the requirements of use. The fitment ratios of the remaining specimens were similar to those of the UHPC used in specimen RS, except that the relevant adjustments were made according to the test variables of the group, as detailed in Table 3.

Table 2. Mix proportions of reference specimen RS (kg/m^3).

Coagulation Material				Quartz Sand	Water	Superplasticizer	Steel Fiber	
Cement	Silica Powder	Fly Ash	Mineral Powder				RS65/8	RS60/13
646	215	108	107	1076	172	14	52	104

Table 3. Specimen details.

Group	Specimen Number	Steel Fiber Content/%	Water/Binder Ratio	Sand Binder Ratio	Curing Condition	Stress Level	f_f/MPa	f_{cu}/MPa
RS	RS	2.0	0.16	1.0	SC	0.3	17.40	129.80
SF	SF-0	0	0.16	1.0	SC	0.3	10.85	81.83
	SF-1.0	1.0					16.07	128.06
	SF-1.5	1.5					19.02	140.35
	SF-2.5	2.5					20.67	145.63
CUR	NC	2.0	0.16	1.0	NC	0.3	18.50	120.30
	HW2				HW2		15.03	140.52
	250DA3				250DA3		15.71	136.20
	HW2-250DA3				HW2-250DA3		20.32	156.52
WBR	WBR-0.14	2.0	0.14	1.0	SC	0.3	15.03	130.41
	WBR-0.18		0.18				19.22	137.26
	WBR-0.20		0.20				14.67	123.40
SBR	SBR-0.9	2.0	0.16	0.9	SC	0.3	20.02	143.23
	SBR-1.1			1.1			19.41	148.75
	SBR-1.2			1.2			11.03	86.20
SL	RS/0.2	2.0	0.16	1.0	SC	0.2	17.40	129.80
	NC/0.2						18.50	120.30
	SBR-0.9/0.2						20.02	143.23
	SBR-1.1/0.2						19.41	148.75
	SBR-1.2/0.2						11.03	86.20

To determine UHPC's cubic compressive strength (f_{cu}) and flexural strength (f_f) for each specimen, three cubic specimens (100 × 100 × 100 mm) and three flexural specimens (100 × 100 × 400 mm) were cast simultaneously. The flexural strength (f_f) provided a reference for loading the specimen at the appropriate stress level.

2.2. Design of Specimen

The research methodology followed for the present study is presented in Figure 1 with the help of a flow chart. A total of 20 UHPC small beams were designed, with dimensions of 100 × 100 × 400 mm and a clear span of 300 mm. Based on the test variables, six groups of specimens were created.

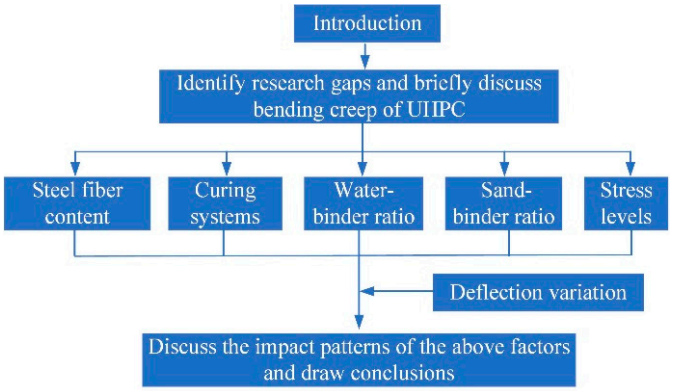

Figure 1. The research methodology followed in the present study.

The reference specimens, designated as Group 1 (RS) specimens, comprised a single specimen bearing the specimen named RS. Group 2's (SF) test variable was steel fiber content and the group contained 4 specimens. The specimens were named SF-0, SF-1,

SF-1.5, and SF-2.5, respectively, and steel fiber content was 0, 1%, 1.5%, and 2.5%. Group 3's (CUR) test variable was the curing system, and the group contained 4 specimens. The following four curing systems were established: (1) natural curing, (2) hot water curing (two days of hot water curing at 90 °C; then, placed under natural environment to the desired age after completion), (3) dry heat curing (three days of dry heat curing at 250 °C; then, placed under natural environment to the desired age after completion), and (4) hot water and dry heat combined curing (two days of hot water curing at 90 °C and then three days of dry heat curing at 250 °C, followed by being placed under natural environment to the desired age after completion). The specimen numbers NC, HW2, 250DA3, HW2-250DA3 corresponded to the four distinct curing regimens mentioned above. Group 4's (WBR) test variable was the water/binder ratio, which contained three specimens with water/binder ratio ratios of 0.14, 0.18, and 0.20, with specimens named WBR-0.14, WBR-0.18, and WBR-0.20, in this order. The test variable for Group 5 (SBR) was the sand/binder ratio, which consisted of three specimens with sand/binder ratios of 0.9, 1.1, and 1.2, and the specimens were named SBR-0.9, SBR-1.1, and SBR-1.2, respectively. The stress level of the specimens for the above five groups was 0.3. The sixth group of test variables comprised stress level (SL), and all stress levels were 0.2, containing five specimens. The specimens were named RS/0.2, NC/0.2, SBR-0.9/0.2, SBR-1.1/0.2, and SBR-1.2/0.2, in this order.

Except for the Group 3 (CUR) specimens, all specimens were cured using standard curing (SC), which means they were immediately placed in a standard curing room with a temperature of 20 ± 2 °C and a relative humidity of over 95% after demolding. Details of the test specimens are shown in Table 3.

2.3. Loading and Measurement Scheme

The UHPC bending creep test used a spring loading device designed according to Hooke's law, as shown in Figure 2. The device applies a load to a specimen by compressing the spring, ordering the spring with a pre-given spring stiffness, and controlling the amount of stress by controlling spring compression deformation. The small size of the device and the negligible temperature-induced error satisfied the need for large-volume durability testing in a short period of time.

Figure 2. Test loading device.

Before loading, the flexural strength of different specimens was tested. Every specimen had a clear span of 300 mm and was only supported at both ends. The micrometer's magnetic table holder was positioned appropriately, and the deflection value of the beam in the span was measured using the device, whose configuration is depicted in Figure 3. Additionally, a temperature and humidity recorder were employed to document the variations in temperature and humidity at the loading site over time.

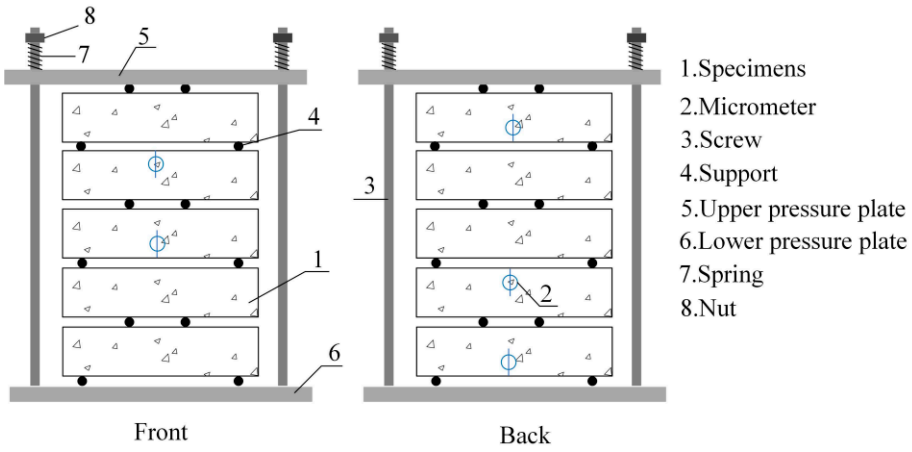

Figure 3. Dial indicator arrangement.

3. Test Results

After all specimens were cured for 28 days, a bending creep test was carried out for 445 days. Temperature and humidity recorders were used to record the change rule of temperature and humidity with time at the loading site, as shown in Figure 4. The test had an average temperature of 20.4 °C and an average humidity of 33.4%. A micrometer was used to record the variation rule of the mid-span deflection of the UHPC beam specimen with time. The results are displayed in Table 4.

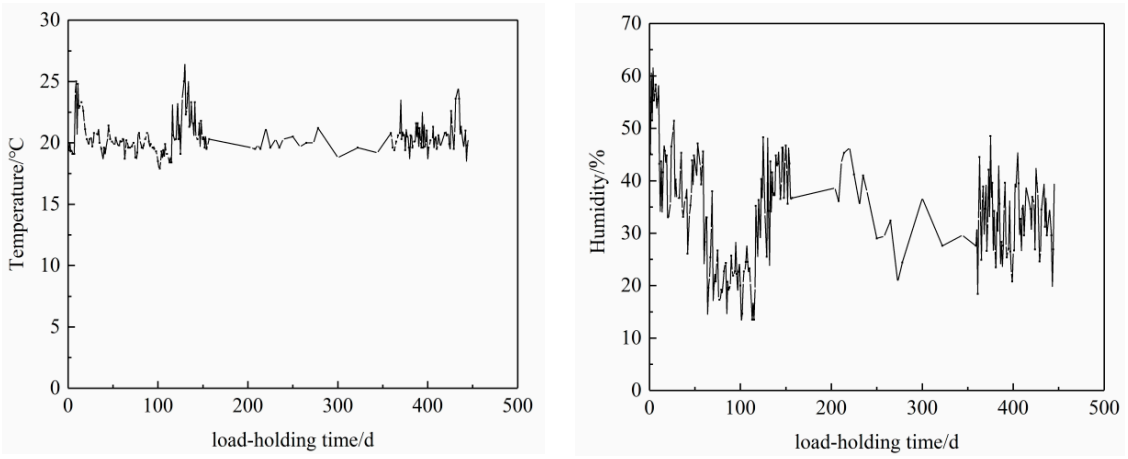

Figure 4. Curves of temperature and humidity. (**a**) Temperature variation curve. (**b**) Humidity change curve.

The deflection creep coefficient θ was defined to characterize the effect brought about by the specimens' creep.

$$\theta = f_c / f_0 \quad (1)$$

$$f = f_0 + f_c \quad (2)$$

where f_0 represents the initial deflection after loading, f_c represents the creep deflection resulting from long-term load bearing, and f represents the total deflection, which is the sum of the initial and creep deflections.

Table 4. Measured deflection of the specimen under 445 days loading.

Group	Specimen Number	f_0/mm	f_c/mm	f/mm	θ	Completion Days/d	
						50% θ	90% θ
RS	RS	0.039	0.276	0.315	7.077	300	414
SF	SF-0	0.072	0.221	0.293	3.069	142	231
	SF-1.0	0.047	0.199	0.246	4.234	265	410
	SF-1.5	0.022	0.273	0.295	12.409	273	388
	SF-2.5	0.059	0.374	0.433	6.339	232	366
CUR	NC	0.053	0.538	0.591	10.151	204	415
	HW2	0.047	0.311	0.358	6.617	250	400
	250DA3	0.121	0.501	0.622	4.140	181	415
	HW2-250DA3	0.034	0.357	0.391	10.500	305	403
WBR	WBR-0.14	0.037	0.243	0.280	6.568	300	401
	WBR-0.18	0.056	0.429	0.485	7.661	204	395
	WBR-0.20	0.108	0.504	0.612	4.667	153	413
SBR	SBR-0.9	0.038	0.454	0.492	11.947	310	398
	SBR-1.1	0.054	0.638	0.692	11.815	315	419
	SBR-1.2	0.161	0.538	0.699	3.342	189	405
SL	RS/0.2	0.033	0.215	0.248	6.515	322	419
	NC/0.2	0.058	0.458	0.516	7.897	157	399
	SBR-0.9/0.2	0.030	0.207	0.237	6.900	312	409
	SBR-1.1/0.2	0.077	0.414	0.491	5.377	290	382
	SBR-1.2/0.2	0.069	0.490	0.559	7.101	306	403

4. Analysis of Influencing Factors

4.1. Steel Fiber Content

The effect of different steel fiber doping rates on the flexural creep of UHPC is shown in Figure 5. Among them, Figure 5a shows the deflection time course curves of specimen deflection development with time for different steel fiber volume doping rates, and Figure 5b shows the deflection development ratio for different specimens.

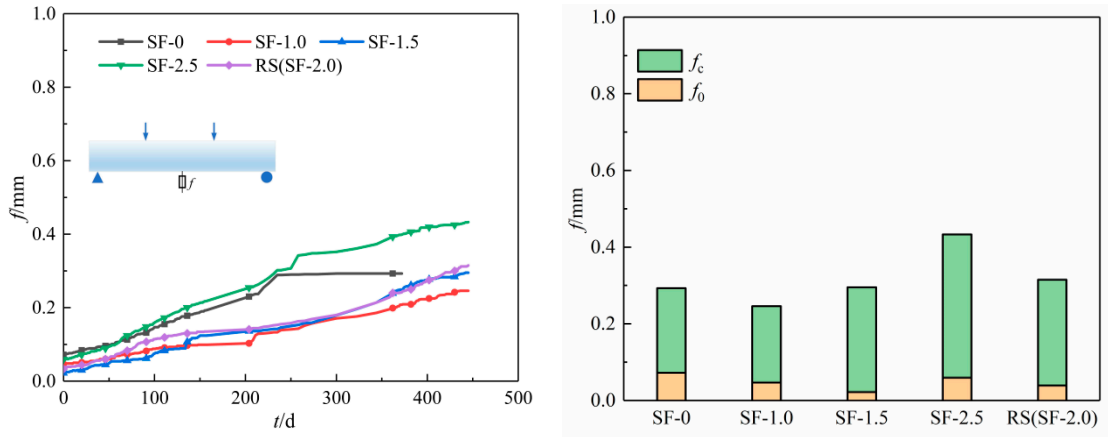

(**a**) (**b**)

Figure 5. Influence of steel fiber content on bending creep. (**a**) Deflection time course curve. (**b**) Deflection development ratio.

The initial deflection of SF-1.0, SF-1.5, RS (2%, steel fiber content), and SF-2.5 decreased by 34.72%, 69.44%, 45.83%, and 18.05%, respectively, when compared to specimen SF-0, as shown in Figure 5. Creep deflection increased by −9.95%, 23.53%, 24.89%, and 69.23%, respectively. The specimens' initial deflection dropped, their creep deflection increased,

and their total deflection first decreased and subsequently increased when the steel fiber doping rate increased. As a result, the specimens' initial deflection was visibly inhibited by the steel fiber. Remarkably, SF-0, devoid of steel fibers, exhibits the greatest initial deflection and the quickest rate of deflection growth; in total, 50% of the overall creep process (445 days) was completed in 142 days, and the fracture happened at 300 day of loading age. The biggest initial and creep deflections were found in SF-2.5, suggesting that an excess of steel fibers may lessen their ability to limit the creep of UHPC.

Steel fibers with a high modulus of elasticity and high tensile strength had good interfacial bonding with UHPC, which can significantly improve the connection, deformation, and cracking resistance of the hardened slurry. The hardened matrix of UHPC was prone to shrinkage and creep under load. By causing deformation and bonding slip, steel fibers added to UHPC can absorb energy, reallocate stress within the microstructure, and prevent UHPC from creeping or shrinking. Excessive steel fiber integration, though, may lessen this capability. This was due to the low UHPC water/binder ratio and the fact that adding more steel fiber dose decreased the fluidity of newly mixed UHPC. This led to a weaker interfacial transition zone between the steel fibers and the matrix and more new defects in the UHPC, which partially offset the creep inhibition effect of the steel fibers. Nevertheless, the mechanical characteristics of UHPC were diminished when the volume doping rate of steel fibers was less than 1%, since the steel fibers were unable to effectively form a mesh to enhance the matrix microstructure. As a result, UHPC's steel fiber doping level has to fall within a suitable range. In conjunction with the test findings, 1–2% steel fiber content in UHPC was recommended.

4.2. Maintenance System Curing Systems

The effect of different maintenance regimes on the flexural creep of UHPC is shown in Figure 6, wherein Figure 6a shows the deflection time course curves of the specimen deflection development with time for different maintenance regimes, and Figure 6b shows the proportion of deflection development for different specimens.

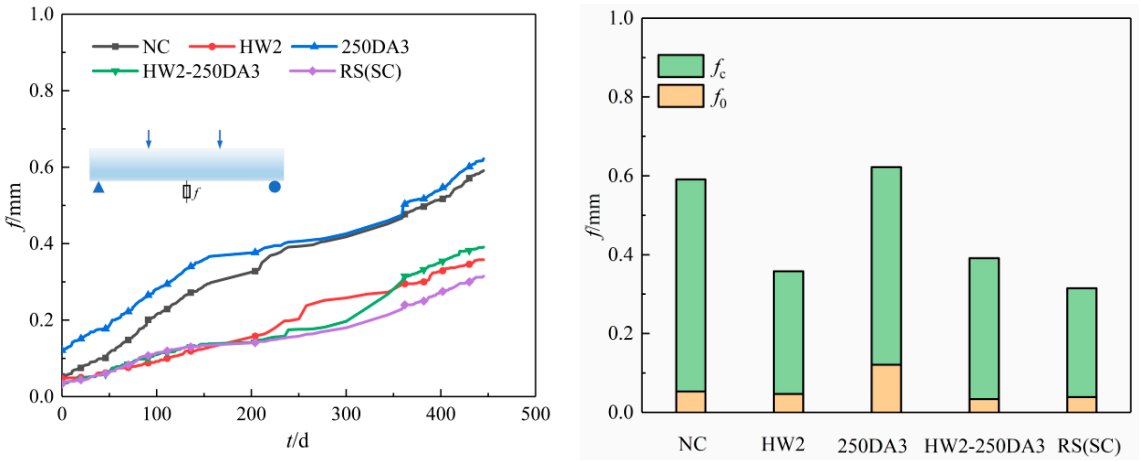

Figure 6. Influence of curing system on bending creep. (**a**) Deflection time course curve. (**b**) Deflection development ratio.

As can be seen from Figure 6, compared with specimen NC, the initial deflections of HW-2, 250DA3, HW2-250DA3, and RS were reduced by 11.32%, −128.30%, 35.85%, and 26.42%, respectively; the creep deflections were reduced by 42.19%, 6.88%, 33.64%, and 48.70%; the total deflections were sequentially reduced by 39.42%, −5.25%, 33.84%, and 46.70%; and the deflection creep coefficient was reduced by 34.81%, 59.21%, −3.44%, and 30.28%. It can be seen that the initial deflection of HW2-250DA3 was the smallest, RS's creep deflection was the smallest, the initial deflection and creep deflection of NC and

250DA3 were the highest, and the creep development rate was faster. It only took 204 days and 181 days, respectively, to complete 50% of the total creep process (445 days).

Heat treatment during the curing stage could effectively reduce the shrinkage of the concrete material in the later stage, while the concrete would continue to shrink in the later stage after the completion of natural curing. Heat treatment was used to speed up hydration and modify the concrete matrix's microstructure during the curing stage. This microstructure refinement was most noticeable near the fibers. The fiber–matrix interface's improved structure and characteristics had a higher ability to prevent UHPC shrinkage and creep in later phases. Without a heat treatment of UHPC, the casting process may form a water film around the fibers, leading to a higher local water/binder ratio. Heat treatment could promote a further reaction of the cement paste, leading to a reduction in porosity around the fibers and an improvement in fiber–matrix interface defects.

In addition to the binding water found in the material, a significant amount of water was needed for the rehydration of concrete, and this water needed to originate from the surrounding environment. Even though the heat treatment could accelerate the hydration reaction, if the UHPC hydration response was insufficient, a shortage of water during the curing process could also lead to an increase in creep. For instance, NC and 250DA3 did not have access to a water environment during the curing, and they exhibited high initial and creep deflections as well as a rapid rate of creep development. By using hot water at 90 °C for just two days, HW2 was able to achieve results that were nearly identical to RS (normal curing for 28 days). This resulted in a significant reduction in curing time and increased labor efficiency, and it may find widespread use in the assembly of components.

4.3. Water/Binder Ratio

The effect of different water/binder ratios on the bending creep of UHPC is shown in Figure 7, wherein Figure 7a shows the deflection time course curves of the deflection development with time for the specimens with different water/binder ratios, and Figure 7b shows the percentage of deflection development for different specimens.

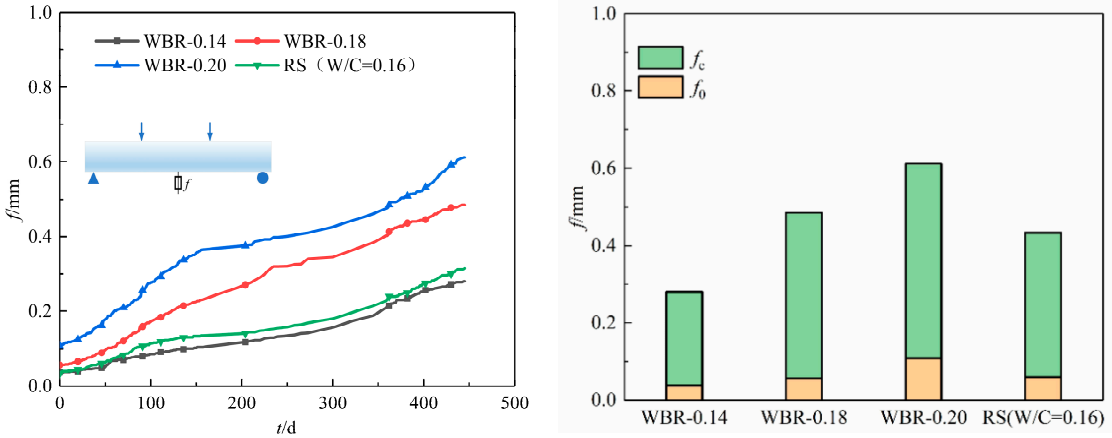

(**a**) (**b**)

Figure 7. Influence of water/binder ratio on bending creep. (**a**) Deflection time course curve. (**b**) Deflection development ratio.

From Figure 7, it can be seen that compared with specimen WBR-0.14, the initial deflection of RS, WBR-0.18, and WBR-0.20 increased by 5.41%, 51.35%, and 191.89%; the creep deflection increased by 13.58%, 76.54%, and 107.41%; the total deflection increased by 12.50%, 73.21%, and 118.57%; and the deflection creep coefficient increased by 7.75%, 16.63%, −28.95%, respectively. It was evident that the specimens' initial deflection, creep deflection, and total deflection all greatly increased as the water/binder ratios grew. The creep deflection of WBR-0.18 and WBR-0.20 developed quickly; in total, 50% of the whole creep process (445 days) was completed in 204 days and 153 days, respectively.

The type and nature of hydration products, porosity, and microstructure can all be strongly impacted by the water/binder ratio. Because more water reacts with cementitious material and produces hydration products, the chemical self-shrinkage of UHPC increases as the water/binder ratio rises. Concurrently, there was a higher potential for creep because of how readily a substantial quantity of free water in UHPC can evaporate. The effect of the water/binder ratio on the creep of UHPC is significant. This study pointed out that the movement of water is one of the most important factors leading to the creep. Moreover, the larger the water/binder ratio, the more free the water remains after the hydration of cement, the greater the evaporation of water from the hardened concrete, the higher the internal porosity, and the greater the creep of UHPC. It can be seen that the water/binder ratio of UHPC should be controlled within a reasonable range, and it is recommended that it should generally not exceed 0.20.

4.4. Sand/Binder Ratio

The effect of different sand/binder ratios on the flexural creep of UHPC is shown in Figure 8, wherein Figure 8a shows the deflection time course curves of the specimen deflection development with time for different sand/binder ratios, and Figure 8b shows the percentage of deflection development for different specimens.

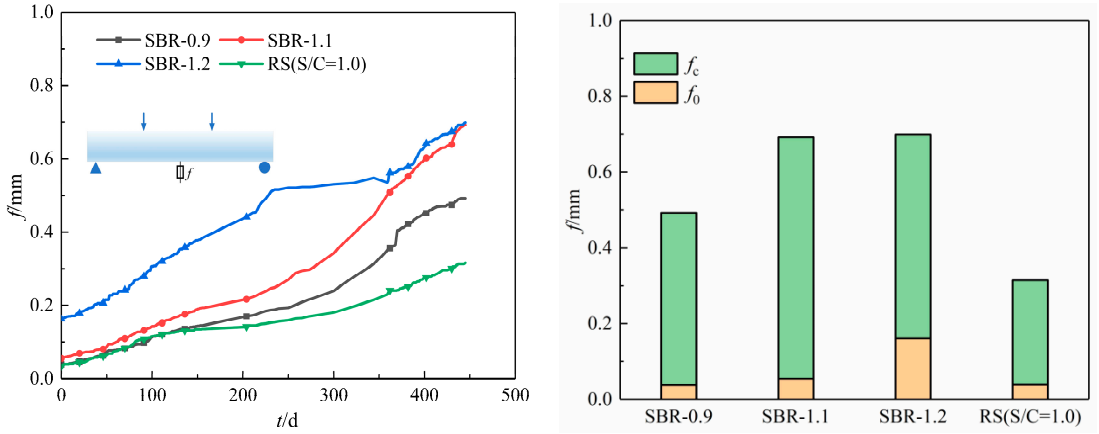

(**a**) (**b**)

Figure 8. Influence of sand/binder ratio on bending creep. (**a**) Deflection time course curve. (**b**) Deflection development ratio.

As observed in Figure 8, the initial deflection of RS, SBR-1.1, and SBR-1.2 increased by 2.63%, 42.11%, and 323.68%, respectively, when compared to specimen SBR-0.9; the creep deflection increased by −39.21%, 40.53%, and 18.50%; the total deflection increased by −35.98%, 40.65%, and 42.07%; and the deflection creep factor decreased by 40.76%, 1.11%, and 72.03%, respectively. It was evident that as the sand/binder ratio rose, the specimens' initial deflection rose along with their creep deflection and total deflection, which first dropped and then increased. SBR-1.2's creep deflection developed at the quickest pace; in total, 50% of the whole creep process (445 d) was completed in just 189 days. It can be seen that the appropriate sand/binder ratio had a certain inhibitory effect on the creep.

In general, the harder the aggregate, the higher the modulus of elasticity. Further, the larger the volume proportion occupied by the aggregate, the smaller the deflection induced by the pressure transferred from the gel flow to the aggregate. Nonetheless, based on test results, the initial deflection and creep deflection increase as the sand/binder ratio increases, with the exception of RS (sand/binder ratios of 1.0). Specimens SBR-0.9, RS, SBR-1.1, and SBR-1.2 maintained the same capacity, and the proportion of cementitious material became smaller and smaller as the sand/binder ratio increased. The calculated cement dosage of specimens SBR-0.9, RS, SBR-1.1, and SBR-1.2 was 679 kg/m^3, 646 kg/m^3, 614 kg/m^3, and 587 kg/m^3, respectively. Additionally, as the cement dosage was decreasing, the

hydration was not sufficient, and the creep increased. This showed that the total amount of cementitious materials and fine aggregates in UHPC and the ratio of the two should be within a reasonable range.

4.5. Stress Levels

The effect of different stress levels on the flexural creep of UHPC is shown in Figure 9, wherein Figure 9a shows the deflection time course curves of the specimen deflection development with time for different stress levels, and Figure 9b shows the percentage of deflection development for different specimens.

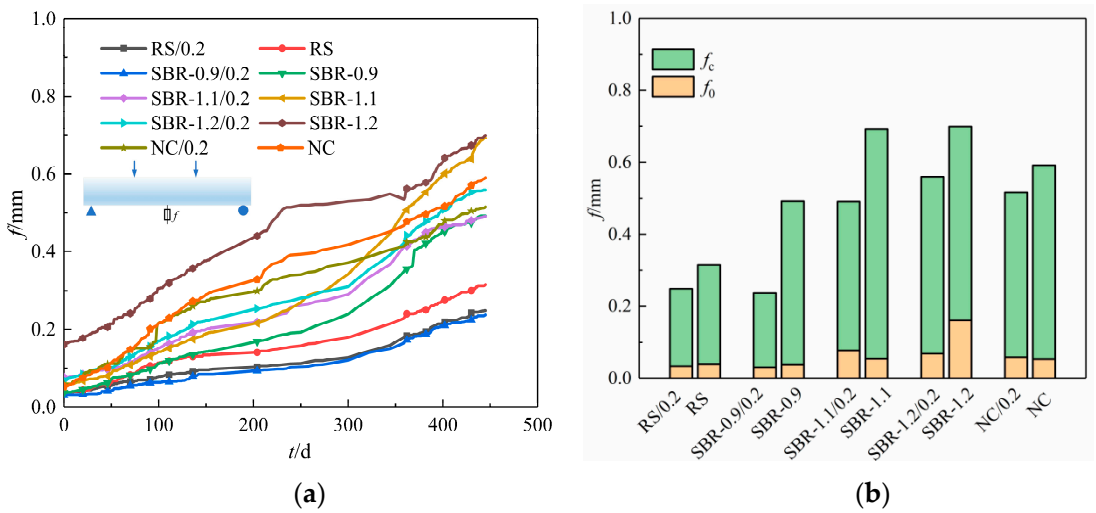

(**a**) (**b**)

Figure 9. Influence of stress level on bending creep. (**a**) Deflection time course curve. (**b**) Deflection development ratio.

From Figure 9, it can be seen that the initial deflections of specimens RS, SBR-0.9, SBR-1.1, SBR-1.2, and NC decreased by 15.38%, 21.05%, −29.87%, 57.14%, and −8.62%, respectively. When the stress levels of specimens RS, SBR-0.9, SBR-1.1, SBR-1.2, and NC were reduced from 0.3 to 0.2, the creep deflections decreased by 22.10%, 54.41%, 35.11%, 8.92%, 14.87%. Consequently, there was a 21.27%, 51.83%, 29.05%, 20.03%, and 12.69% reduction in total deflection, and a 7.94%, 42.25%, 54.49%, −52.94%, 22.20% reduction in the deflection creep coefficient, in this order. It was evident that the specimens' initial deflection, creep deflection, and total deflection all generally increased with the stress level. The rate at which creep developed was also strongly influenced by the stress level. For example, specimens SBR-1.2/0.2 and SBR-1.2 took 306 days and 189 days, respectively, to complete 50% of the total creep process (445 days), whereas specimens NC/0.2 and NC took 157 days and 204 days, respectively, to complete 50% of the total creep process (445 days).

Concrete's creep was directly correlated with its stress level: the higher the stress level, the higher the creep. The gel flowed more quickly, and the pace of creep development became faster as the stress level increased. As a result, selecting a suitable range of pre-stress is essential when employing UHPC for pre-stressing tasks.

5. Conclusions

The deformation properties of 20 UHPC beams under long-term loading were studied in this research study to determine the changes in the beams' deflection patterns for 445 days of continuous loading. The effects of steel fiber content, curing systems, water/binder ratio, sand/binder ratio, and stress level on the deflection of UHPC beams over time were investigated. The following main conclusions were obtained:

(1) With the increase in steel fiber content, the initial deflection of the specimens decreased, the creep deflection increased, and the steel fiber had an obvious inhibiting

effect on the initial deflection of the specimen. However, a dosage of steel fiber too high led to a relatively weak interfacial transition zone between the steel fiber and matrix, which would offset part of the inhibitory effect of the steel fiber on creep, and it was recommended that the dosage rate of the steel fiber in UHPC should be 1~2%.

(2) At the maintenance stage, heat treatment can hasten the hydration effect, leading to improved UHPC shrinkage and creep inhibition later on. NC's and 250DA3's maintenance periods were not provided with a water environment, the initial deflection and creep deflection were very large, and the rate of creep development was fast. Therefore, heat treatment must be coupled with necessary moisture. HW2's curing time was short and efficient, and it can be popularized in the fabrication of assembly components.

(3) The larger the water/binder ratio, the more free the water remaining after cement hydration, the greater the evaporation of water from the hardened concrete, the higher the internal porosity, the greater the creep of UHPC. The water/binder ratio of UHPC should be controlled within a reasonable range, and it is recommended that it should not exceed 0.20 in general.

(4) Both initial and creep deflections increased with an increasing sand/binder ratio, except for RS (sand/binder ratio of 1.0). The total amount of cementitious materials and fine aggregates as well as the ratio of the two should be taken care of in UHPC.

(5) The creep of UHPC had a close relationship with the stress level: the greater the stress level, the greater the creep. Increasing the stress level accelerated the flow of gel and the development rate of creep. Therefore, when UHPC is used in pre-stressing works, a reasonable range of pre-stress should be selected.

Finally, for future research, the authors recommend a comparative study of the variation patterns of compressive creep and bending creep in UHPC under the same size and conditions to be carried out. In addition, it is worth studying the long-term effects of bending creep on the structural integrity of UHPC elements.

Author Contributions: Conceptualization, J.L.; methodology, J.L.; software, Y.L. and X.J.; formal analysis, B.L.; investigation, J.C.; resources, J.L. and B.L.; data curation, Q.M.; writing—original draft preparation, J.L.; writing—review and editing, J.L. and B.L.; visualization, B.L.; supervision, J.L. and B.L. All authors have read and agreed to the published version of the manuscript.

Funding: This research received no external funding.

Data Availability Statement: The data that support the findings of this study are available upon reasonable request from author Jiayue Li.

Conflicts of Interest: The authors declare no conflicts of interest.

References

1. Ranaivomanana, N.; Multon, S.; Turatsinze, A. Tensile, compressive and flexural basic creep of concrete at different stress levels. *Cem. Concr. Res.* **2013**, *52*, 1–10. [CrossRef]
2. Babafemi, A.J.; Boshoff, W.P. Testing and modelling the creep of cracked macro-synthetic fiber reinforced concrete (MSFRC) under flexural loading. *Mater. Struct.* **2016**, *49*, 4389–4400. [CrossRef]
3. Siming, L.; Ya, W. Research on tensile creep model based on degree of hydration for early-age concrete. *Eng. Mech.* **2016**, *33*, 171–177.
4. Pujadas, P.; Blanco, A.; Cavalaro, S.H.P.; De La Fuente, A.; Aguado, A. The need to consider flexural post-cracking creep behavior of macro-synthetic fiber reinforced concrete. *Constr. Build. Mater.* **2017**, *149*, 790–800. [CrossRef]
5. Jahami, A.; Khatib, J.; Raydan, R. Production of low-cost, high-strength concrete with waste glass as fine aggregates replacement. *Buildings* **2022**, *12*, 2168. [CrossRef]
6. Manjunath, M.; Seth, D.; Balaji, K.; Roy, S.; Tangadagi, R.B. Utilization of industrial-based PVC waste powder in self-compacting concrete: A sustainable building material. *J. Clean. Prod.* **2023**, *428*, 139428. [CrossRef]
7. Tailhan, J.; Boulay, C.; Rossi, P.; Le Maou, F.; Martin, E. Compressive, tensile and bending basic creep behaviours related to the same concrete. *Struct. Concr.* **2013**, *14*, 124–130. [CrossRef]
8. Kim, S.G.; Park, Y.S.; Lee, Y.H. Comparison of concrete creep in compression, tension, and bending under drying condition. *Materials* **2019**, *12*, 3357. [CrossRef]
9. Farah, M.; Grondin, F.; Alam, S.; Loukili, A. Experimental approach to investigate creep-damage bilateral effects in concrete at early age. *Cem. Concr. Res.* **2019**, *96*, 128–137. [CrossRef]

10. Berger, J.; Gericke, O.; Feix, J.; Sobek, W. Experimental investigations on actively bent concrete shells. *Struct. Concr.* **2020**, *21*, 2268–2281. [CrossRef]
11. Ding, Y.; Fang, Y.; Jin, W.; Zhang, J.; Li, B.; Mao, J. Numerical method for creep analysis of strengthened fatigue-damaged concrete beams. *Buildings* **2023**, *13*, 968. [CrossRef]
12. Buratti, N.; Mazzotti, C. Experimental tests on the effect of temperature on the long-term behaviour of macrosynthetic fibre reinforced concretes. *Constr. Build. Mater.* **2015**, *95*, 133–142. [CrossRef]
13. Buratti, N.; Ferracuti, B.; Savoia, M. Concrete crack reduction in tunnel linings by steel fibre-reinforced concretes. *Constr. Build. Mater.* **2013**, *44*, 249–259. [CrossRef]
14. Taengua, E.; Arango, S.; Vargas, M. Flexural creep of steel fiber reinforced concrete in the cracked state. *Constr. Build. Mater.* **2014**, *65*, 321–329. [CrossRef]
15. Vrijdaghs, R.; Prisco, M.D.; Vandewalle, L. Sectional analysis of the flexural creep of cracked fiber reinforced concrete. *Struct. Concr.* **2021**, *22*, 1817–1830. [CrossRef]
16. Yazdizadeh, Z.; Marzouk, H.; Hadianfard, M.A. Monitoring of concrete shrinkage and creep using fiber bragg grating sensors. *Constr. Build. Mater.* **2017**, *137*, 505–512. [CrossRef]
17. Zhang, Y.; Zhu, P.; Zhu, Y.; Bao, C.; Shao, X.; Shi, J. NC-UHPC composite structure for long-term creep-induced deflection control in continuous box-girder bridges. *J. Bridge Eng.* **2018**, *23*, 04018034. [CrossRef]
18. Zhu, L.; Wang, J.-J.; Li, X.; Zhao, G.-Y.; Huo, X.-J. Experimental and numerical study on creep and shrinkage effects of ultra high-performance concrete beam. *Compos. Part B* **2020**, *184*, 107713. [CrossRef]
19. Llano, T.A.; Jose Rocio Martí-Vargas Serna, P. Flexural and compressive creep behavior of UHPFRC specimens. *Constr. Build. Mater.* **2020**, *244*, 118254. [CrossRef]
20. Xu, Y.; Liu, J.; Liu, J.; Zhang, P.; Zhang, Q.; Jiang, L. Experimental studies and modeling of creep of UHPC. *Constr. Build. Mater.* **2018**, *175*, 643–652. [CrossRef]
21. Chen, Y.; Liu, P.; Sha, F.; Yu, Z.; He, S.; Xu, W.; Lv, M. Effects of type and content of fibers, water-to-cement ratio, and cementitious materials on the shrinkage and creep of ultra-high performance concrete. *Polymers* **2022**, *14*, 1956. [CrossRef] [PubMed]
22. Zhang, Z.; Xu, T.; Deng, K.; Tong, T.; Zhou, H. Experimental study on creep failure of non-steam-cured ultrahigh-performance concrete under high uniaxial compressive stress. *J. Mater. Civ. Eng.* **2022**, *34*, 04022105. [CrossRef]
23. Zhang, Y.; Zhu, Y.; Xu, Z.; Shao, X. Long-term creep behavior of NC filled UHPC tube composite column. *Eng. Struct.* **2022**, *259*, 114214. [CrossRef]
24. Mohebbi, A.; Graybeal, B.; Haber, Z. Time-dependent properties of ultrahigh-performance concrete: Compressive creep and shrinkage. *J. Mater. Civ. Eng.* **2022**, *34*, 04022096. [CrossRef]
25. Garas, V.Y. Multi-Scale Investigation of Tensile Creep of Ultra-High Performance Concrete for Bridge Applications. Ph.D. Thesis, Georgia Institute of Technology, Atlanta, GA, USA, 2009.
26. Garas, V.Y.; Kurtis, K.E.; Kahn, L.F. Creep of UHPC in tension and compression: Effect of thermal treatment. *Cem. Concr. Compos.* **2012**, *34*, 493–502. [CrossRef]
27. Cui, C. Influence of Curing Regime on Shrinkage, Creep and Basic Mechanical Proper-Ties of Ultra-High Performance Concrete. Master's Thesis, Beijing Jiaotong University, Beijing, China, 2018.
28. Abid, M.; Hou, X.; Zheng, W.; Hussain, R.R.; Cao, S.; Lv, Z. Creep behavior of steel fiber reinforced reactive powder concrete at high temperature. *Constr. Build. Mater.* **2019**, *205*, 321–331. [CrossRef]